Studies on the Trapping and Detrapping Transition States of Atomic Hydrogen in Octasilsesquioxane Using the Density Functional Theory B3LYP Method

Michiko Mattori,[†] Koichi Mogi,*[,‡] Yoshiko Sakai,[‡] and Toshiyuki Isobe[†]

Graduate School of Social and Cultural Studies, Kyushu University, Chuo-ku, Fukuoka, 810-8560, Japan, and Graduate School of Engineering Sciences, Kyushu University, Kasuga-shi, Fukuoka, 816-8580, Japan

Received: April 21, 2000; In Final Form: September 8, 2000

B3LYP level optimizations were performed on the structures of the octasilsesquioxane ($Si_8O_{12}H_8$, HT_8) double four-ring (D4R) cage and single hydrogen atom-trapped HT_8 ($H@HT_8$). Moreover, the transition state in the detrapping process of the hydrogen atom from the D4R cage was examined. The basis sets used were 6-31G** for HT_8 and (3 1 1/1*1*/1*) for the trapped hydrogen atom. Both HT_8 and $H@HT_8$ were structure-optimized with O_h molecular symmetry and the resulting cage conformations were similar. The trapped H atom was located at the center of the D4R cage. The weak interaction between the D4R cage and the trapped H atom in $H@HT_8$ was determined by examining the singly occupied molecular orbital (SOMO) [$8a_{1g}$] of $H@HT_8$. The SOMO was constructed from an antibonding interaction between the lowest unoccupied molecular orbital (LUMO) [$8a_{1g}$] of HT_8 and the 1*s* orbital of the trapped H atom. For the transition state, the structure was optimized with C_{4v} molecular symmetry. As a result, the position of the Si_8 cube framework was unchanged, and four O atoms in a silicon single four-ring were displaced, thereby opening one of the oxygen windows of the D4R cage. The detrapping H atom was located near the center of the oxygen window and the MO illustrations showed a change in shape from spherical to ellipsoid. Consequently, it is clear that the detrapping process is not due to the formation of chemical bonding. The calculated activation and reaction energies of this detrapping process were +98.6 and −26.1 kJ/mol, respectively. In addition, single-point calculations at the MP2 level were done for each optimized structure, and the obtained activation and reaction energies were +128.7 and −9.3 kJ/mol, respectively. Both calculated activation energies were comparable to Stösser's experimental data (+109.6 ± 3.1 kJ/mol) for H•:$Si_8O_{12}(OSi(CH_3)_3)_8$ (Q_8M_8). Furthermore, additional explanations are given on the IR vibrational frequencies of HT_8 and $H@HT_8$ and the hyperfine coupling constant for caged atomic hydrogen by ESR.

Introduction

A double four-ring (D4R) structure is one of the secondary building units (SBUs) in zeolite frameworks. Small clathrasils, such as $Si_8O_{12}H_8$ (HT_8),[1] $Si_8O_{12}(CH_3)_8$ (MeT_8),[2] and Si_8O_{12}-$(OSi(CH_3)_3)_8$ (Q_8M_8),[3] with an empty cage-like structure have been synthesized as porous all-silica materials or porosils.[4] Figure 1 shows the structures and denominations of these octasilsesquioxanes ($Si_8O_{12}R_8$). Several years ago, Matsuda et al.[5,6] reported interesting features of the D4R silicate cage. Measuring ESR spectra, they found that the D4R cage stably encapsulates atomic hydrogen in both solution and crystal at room temperature on γ-ray irradiation of the crystal. Subsequently, Päch and Stösser [7] estimated the activation energy for the thermal decay process of H• trapped in the solid state to be +109.6 ± 3.1 kJ/mol (343 K ≤ *T* ≤ 387 K) in the case of Q_8M_8.

On the other hand, there have been several theoretical studies of the D4R cages.[8−11] George and Catlow [12] investigated the effects of ion incorporation on the D4R, when an F^- anion, a Na^+ cation, or an OH^- anion was introduced into the center of the D4R cage. It was shown that this also produces an appreciable change in electron density or perturbation in the geometry. In a computational study, Tossell [13] studied the inclusion of Ti^{4+} and Zr^{4+} in the center of the D4R cage of aluminosilicates and borosilicates. Xiang et al.[10] reported the results for H-silsesquioxane cages (i.e., $(HSiO_{3/2})_n$ (designated as T_n) with $n = 4$, 6, 8, 10, 12, 14, and 16). They presented the spatial extent (the contour pictures) of the highest occupied molecular orbitals (HOMOs) and lowest unoccupied molecular orbitals (LUMOs) for T_8 (O_h) and T_{16} (D_{2d}). The above-mentioned studies were done according to Hartree−Fock (HF) theory, except Xiang et al.[10] used the local density approximation (LDA) and nonlocal density approximation (NDLA) levels and Jug[11] used the semiempirical MSINDO method.

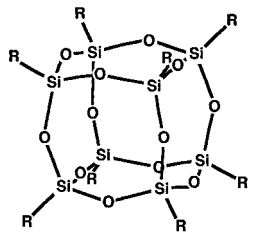

R = H (HT_8), CH_3 (MeT_8) and $OSi(CH_3)_3$ (Q_8M_8).

Figure 1. Structures and denominations of octasilsesquioxanes ($Si_8O_{12}R_8$).

In this work, we report the results of calculations on HT_8 itself, and the trapping and detrapping transition states of atomic hydrogen in HT_8, focusing on the activation energy of the detrapping process of atomic hydrogen. The significance of these

* E-mail: mogi@mm.kyushu-u.ac.jp.
[†] Graduate School of Social and Cultural Studies, Kyushu University.
[‡] Graduate School of Engineering Sciences, Kyushu University.

10.1021/jp0015269 CCC: $19.00
Published on Web 11/01/2000

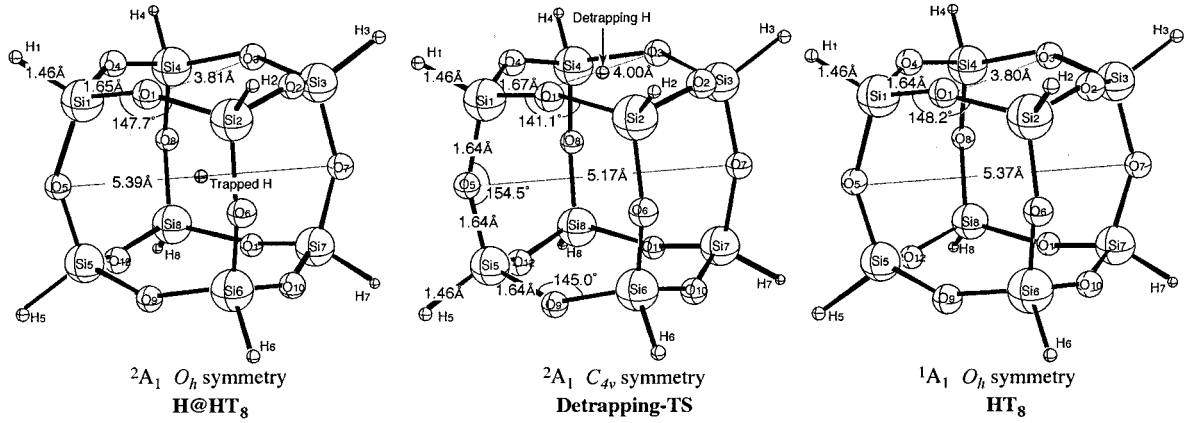

Figure 2. Optimized structures for H@HT$_8$, Detrapping-TS, and HT$_8$.

calculations lie in (1) comparison of the available experimental structural, vibrational, and electron spin resonance (ESR) data for such states and (2) computational estimation of the physicochemical quantities of the transition state (TS), which are difficult to measure. The optimized structure and the molecular orbital (MO) are also illustrated. Specifically, we employed density functional theory (DFT) as a computational methodology,[14] because for the sake of estimating the energy and structure of the transition state, it is desirable to use a method that considers electron correlation effects. Calculations using the Møller−Plesset perturbation method were also attempted by way of single-point calculations. In addition to the structural and energetic properties, we calculated the infrared (IR) vibrational frequencies and hyperfine coupling constant of caged atomic hydrogen in ESR.

Computational Methods

The hybrid density functional theory (DFT) method based on Becke's 3 parameter functional with nonlocal correlation provided by the Lee, Yang, and Parr functional (LYP), designated as B3LYP,[15] is used. The B3LYP functional is expressed in the following form:

$$E^{(\mathrm{B3LYP})} = AEx^{(\mathrm{Slater})} + (1 - A)Ex^{(\mathrm{HF})} + BEx^{(\mathrm{Becke})} + CEc^{(\mathrm{LYP})} + (1 - C)Ec^{(\mathrm{VWN})} \quad (1)$$

where the respective energy terms are the Slater exchange, the Hartree−Fock exchange, Becke's 1988 exchange functional correction, the gradient-corrected correlation functional of Lee, Yang and Parr, and the local correlation functional of Vosko, Wilk and Nusair. *A*, *B*, and *C* are semiempirical coefficients determined by an appropriate fitting to a Gaussian-1[16,17] molecule set: $A = 0.80$, $B = 0.72$, and $C = 0.81$. The geometry optimizations and frequency calculations were performed with O_h symmetry for HT$_8$ and H@HT$_8$ as the initial configuration, and with C_{4v} symmetry for the transition state. The optimized structures of HT$_8$ and H@HT$_8$ have been identified as the minimum (number of imaginary frequencies, NIMAG, = 0) and that of the transition state, as the saddle point (NIMAG = 1). Furthermore, single-point calculations were done by the Møller−Plesset second-order perturbation (MP2) method[18] for the optimized geometry obtained by the B3LYP level calculation to determine the activation energy for the detrapping process of atomic hydrogen. All of these calculations were carried out with the 6-31G** basis set [19,20] for HT$_8$, and the valence triple-ζ basis set augmented with two *p*- and one *d*-type polarization functions, (3 1 1/1*1*/1*),[21,22] for the trapped hydrogen atom, specifically to take the interaction between the HT$_8$ cage and the trapped H (named Basis I) into account. Zero-point vibrational corrections were made for the calculations of activation and reaction energies of the detrapping process.

Spin density at the nucleus ($\rho(0)$) of the trapped hydrogen and isotropic hyperfine coupling constant (A_0) were calculated at unrestricted Hartree−Fock (UHF),[23] B3LYP, and MP2 levels (UHF/Basis I//UHF/Basis I, B3LYP/Basis I//B3LYP/Basis I, and MP2/Basis I//B3LYP/Basis I). Next, Basis I was modified further and single-point calculations were performed at the three levels in the following way. Matsuoka's triple-ζ basis set[24] augmented with two *p*- and one *d*-type polarization functions,[22] (13 1 1/1*1*/1*), named Basis II, was applied for the trapped hydrogen atom. Using Basis II, the values of $\rho(0)$ were estimated by way of single-point calculations at UHF and B3LYP levels for the structures optimized with Basis I at each level (UHF/Basis II//UHF/Basis I and B3LYP/Basis II//B3LYP/Basis I). MP2 single-point calculations were made for the structure that was optimized with Basis I at the B3LYP level (MP2/Basis I//B3LYP/Basis I and MP2/Basis II//B3LYP/Basis I). The spin density of the free hydrogen atom as a collation measure was calculated by the UHF method. All calculations were performed with the GAUSSIAN 98 program package.[25]

Results and Discussion

Structures. Three stationary points were optimized as shown in Figure 2. The optimized structural parameters are given in Table 1 together with the experimental parameters for HT$_8$ obtained by X-ray crystal structure analysis at 100 K.[26] It is reported that the ideal O_h symmetry for the D4R framework of HT$_8$ is only realized in solution. Each of the ^{1}H and ^{29}Si nuclear magnetic resonance (NMR) spectra consists of a single peak, and the IR spectrum is consistent with the O_h point group in carbon tetrachloride.[27] On the other hand, the effective T_d symmetry shown in the crystal, indicated by the clear difference between the O−O distances across the faces of the Si$_8$ cube (∼0.31 Å; see Table 1), is a consequence of the crystal packing.

In this study, the structure of HT$_8$ was optimized by specifying the $^1A_1$ electronic state with O_h molecular symmetry shown in the right-hand side of Figure 2. In the O_h symmetry approximation, the positions of Si and O are completely determined with only two parameters: bond length Si−O and bond angle ∠(Si−O−Si). The calculated bond length Si_1-O_1 and bond angle ∠($Si_1-O_1-Si_2$) was 1.64 Å and 148.1°, respectively. These values are slightly longer (∼0.02 Å) and larger (0.7°) than those of crystalline HT$_8$ with effective T_d symmetry. The O_5-O_7 distance (5.37 Å) is regarded as a measure of the size of the cavity in the D4R cage and the O_1-O_3 distance (3.80 Å) as a measure of the so-called oxygen

TABLE 1: Optimized Structural Parameters for Each State

	calcd			exp
	H@HT$_8$	**TS**	**HT$_8$**	**HT$_8$**[a]
symmetries	O_h	C_{4v}	O_h	effective T_d
	Distances (Å)			
Si_1-O_1	1.65	1.67	1.64	1.6195
Si_1-O_5	1.65	1.64	1.64	1.6185
Si_5-O_5	1.65	1.64	1.64	1.6191
Si_5-O_9	1.65	1.64	1.64	1.6168
Si_1-H_1	1.46	1.46	1.46	
Si_5-H_5	1.46	1.46	1.46	
O_1-O_3	3.81	4.00	3.80	3.5752
O_9-O_{11}	3.81	3.81	3.80	3.8826
O_5-O_7	5.39	5.17	5.37	
O_1-O_{11}	5.39	5.53	5.37	
Si_1-Si_2	3.16	3.15	3.16	3.1085
Si_5-Si_6	3.16	3.14	3.16	3.1075
Si_1-Si_3	4.47	4.45	4.47	
Si_5-Si_7	4.47	4.44	4.47	
Si_1-Si_7	5.48	5.48	5.48	5.3901 5.3809
Si_n−the center of the cage	2.74		2.74	
O_n−the center of the cage	2.69		2.68	
Si_1−the center of the (O_5,O_6,O_7,O_8) plane		2.74		
O_1−the center of the (O_5,O_6,O_7,O_8) plane		2.79		
Si_1−atomic H		2.27		
O_1−atomic H		2.00		
	Angles (deg)			
$Si_1-O_1-Si_2$	147.7	141.1	148.2	147.49
$Si_1-O_5-Si_5$	147.7	154.5	148.2	147.60
$Si_5-O_9-Si_6$	147.7	145.0	148.2	
$O_1-Si_1-O_4$	109.8	115.9	109.6	109.48
$O_1-Si_1-O_5$	109.8	108.3	109.6	109.66
$O_5-Si_5-O_9$	109.8	109.5	109.6	109.45
$O_9-Si_5-O_{12}$	109.8	109.8	109.6	109.41
$O_1-Si_1-H_1$	109.1	107.0	109.3	
$O_5-Si_1-H_1$	109.1	110.1	109.3	
$O_5-Si_5-H_5$	109.1	109.5	109.3	
$O_5-Si_5-H_9$	109.1	109.2	109.3	
O_5−atomic H−O_7	180.0			
O_1−atomic H−O_3		175.3		

[a] Reference 26.

windows of the D4R cage. A space-filling representation of the structure modeled using the ionic radii for Si^{4+} and O^{2-} and the atomic radius for trapped H[28] reveals that the D4R cavity has sufficient space to trap a hydrogen atom. The trapped hydrogen atom cannot escape from the oxygen four-ring windows of the D4R cage with this steric hindrance.

Then, the structure of H@HT$_8$ was optimized by specifying the $^2A_1$ electronic state with O_h molecular symmetry as shown in the left-hand side of Figure 2. The D4R cage structure of H@HT$_8$ was very similar to that of HT$_8$ and the trapped H atom was located at the center of the D4R cage. Closely examining Table 1, shows that the calculated bond length Si_1-O_1 and bond angle $\angle(Si_1-O_1-Si_2)$ of H@HT$_8$ are slightly longer (∼0.01 Å) and smaller (∼0.5°) than those of HT$_8$, respectively. There is no change in the Si_1-Si_2 distance, while the O_1-O_3 distance of H@HT$_8$ is slightly longer than in HT$_8$. The O_5-O_7 and O_1-O_3 distances are also slightly longer by ∼0.02 Å and ∼0.01 Å, respectively. As indicated in Table 1, the distance from the Si atoms to the center of the cage is the same (2.74 Å) in HT$_8$ and H@HT$_8$. However, the distance from the O atoms to the center of the cage is slightly longer in H@HT$_8$ (2.69 Å) than in HT$_8$ (2.68 Å). Therefore, the silicon cage remains essentially unchanged upon trapping of an H atom, but the bridging oxygen atoms move slightly away from the trapped H atom.

The transition state (TS) structure of the detrapping H atom from H@HT$_8$ was optimized by specifying the $^2A_1$ electronic state with C_{4v} molecular symmetry shown in the center of Figure 2. The detrapping H atom was located at a position on the C_{4v} axis shifted slightly from the center of the oxygen window to the outside of the cage ($\angle(O_1-$atomic H$-O_3) = 175.3°$). The vibrational frequency analysis indicated one imaginary frequency (a_1, 770i cm^{-1}). Therefore, the above-calculated state is identified as a saddle point. In comparison with the TS and the two minimums (HT$_8$ and H@HT$_8$), the detrapping-transition state has almost the same Si−Si distance, with longer O_1-O_3, O_1-O_{11}, and shorter O_5-O_7 distances. In other words, the Si_8 cube structure is almost unchanged, but an oxygen four-ring window is enlarged and the O−detrapping H distance is shortened. These results suggest that considering the O_1-O_3 or O_1-atomic H distance, the detrapping atomic H radius must become smaller than the trapped H radius for the sake of detrapping the H atom.

Electronic Structures and Molecular Orbitals. Figure 3 illustrates both the singly occupied molecular orbitals (SOMOs) for H@HT$_8$ and the TS, and the lowest unoccupied molecular orbital (LUMO) of HT$_8$. The LUMO of HT$_8$ and the SOMO of H@HT$_8$ both correspond to the $8a_{1g}$ orbital. The LUMO of HT$_8$ was characterized by the negative *p*-type lobes of the O atoms facing toward the center of the D4R cage. On the other hand, the SOMO of H@HT$_8$ was constructed from the LUMO of HT$_8$ and the positive 1*s* atomic orbital (AO) of the trapped H atom. Since the *p*-type lobes of the O atoms and the *s*-type AO of the H atom are in the opposite phase, antibonding interactions occur among them. However, in the case of the SOMO of TS, every *p*-type lobe of one four-membered oxygen window faces the detrapping H atom, as illustrated in the center of Figure 3. The shape of the detrapping H atom becomes ellipsoid. There is no

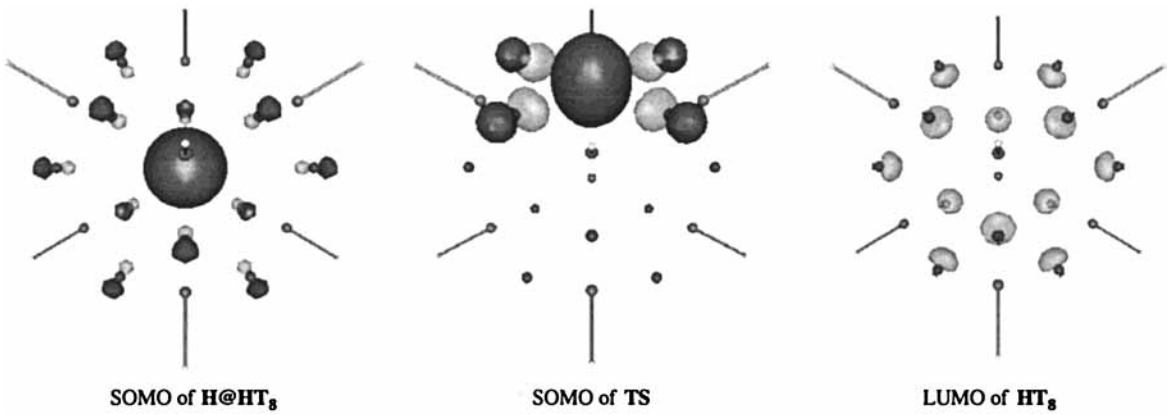

Figure 3. The SOMOs of H@HT$_8$ and TS and the LUMO of HT$_8$. The dark shaded MOs indicate positive phases and the light shaded ones, negative phases.

TABLE 2: IR Fundamentals of HT_8 with Assignments for O_h Symmetry

	HT_8			$H@HT_8$	
type of vibration[a]	frequencies[b,c]	intensities[d]	exp frequencies[c,e]	frequencies[b,c]	intensities[d]
Si−H stretch	2269	355	2277	2267	362
Si−O−Si asym stretch	1108	2130	1141	1099	1987
Si−H bend	862	572	881	857	562
Si breathing	537	25	566	534	10
Si−O−Si bend	433	136	465	477	75
Si−O−Si bend				418	91
Si−O−Si bend	377	174	399	376	174

[a] Reference 9. [b] Scaling factor = 0.9614. Reference 29. [c] IR frequencies in cm^{-1}. [d] IR freqencies in cm^{-1}. [e] In CCl_4. Reference 27.

TABLE 3: Spin Density at Nucleus (ρ(0)/a.u.), Isotropic Hyperfine Coupling Constant (A_0/MHz), and Total Spin Density for the Trapped H Atom (ρ(total)/a.u.)

	$\rho(0)$		A_0		
methods	**H@HT$_8$**	free H atom	**H@HT$_8$**	free H atom	ρ(total)
UHF/Basis I//UHF/Basis I	0.31733	0.28751[a]	1418.4	1285.0[a]	0.986
UHF/Basis II//UHF/Basis I	0.34768	0.31745[a]	1554.0	1418.9[a]	0.966
B3LYP/Basis I//B3LYP/Basis I	0.30259	0.28751[a]	1352.5	1285.0[a]	0.911
B3LYP/Basis II//B3LYP/Basis I	0.31655	0.31745[a]	1414.9	1418.9[a]	0.884
MP2/Basis I//B3LYP/Basis I	0.30264	0.28751[a]	1352.7	1285.0[a]	0.946
MP2/Basis II//B3LYP/Basis I	0.32923	0.31745[a]	1471.6	1418.9[a]	0.938
exp	0.31509[b]	0.31778[c]	1408.4[b]	1420.4057[c]	

[a] The ρ(0) and A_0 of the free hydrogen atom are calculated by the UHF method because that there is no electron correlation. [b] Reference 6. [c] Reference 31.

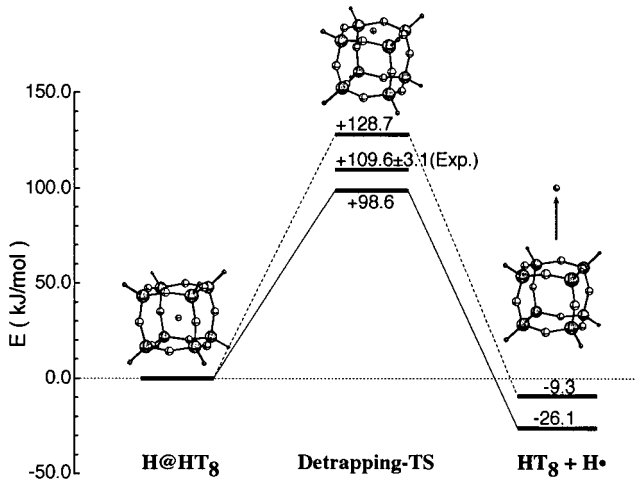

Figure 4. Energy diagram for the detrapping process of atomic hydrogen from $H@HT_8$. Solid lines are B3LYP level optimizations and dashed lines are MP2 level single-point calculations. All structures are optimized with B3LYP/Basis I.

chemical bond between the trapped H atom and the HT_8 cage during the detrapping process according to these MO analyses.

Detrapping Activation and Reaction Energies. Figure 4 shows the correlation energy diagrams for the detrapping process calculated by the B3LYP and MP2 methods. The activation energy of the detrapping process was calculated as +98.6 kJ/mol using B3LYP and +128.7 kJ/mol using MP2. Judging from these values, the process of detrapping an H atom seems to be very difficult. In comparison with Stösser's experimental data (+109.6 ± 3.1 kJ/mol at 343 K ≤ T ≤ 387 K) for $H@Q_8M_8$, B3LYP underestimated the activation energy and MP2 overestimated it. Nevertheless, both obtained values are reasonable.

$H@HT_8$ is located on a higher energetic point than the separated $HT_8 + H^\bullet$ system. The reaction energy was calculated to be −26.1 kJ/mol using B3LYP and −9.3 kJ/mol using MP2; MP2 yielded a particularly small reaction energy. The obtained small positive trapping energy is probably reasonable for the encapsulation of atomic hydrogen.

IR Vibrational Frequencies. The calculated IR frequencies and their relative intensities for HT_8 and $H@HT_8$ are given in Table 2 together with the experimental data for HT_8 in CCl_4. On the basis of the O_h symmetry, the 78 vibrational degrees of freedom of HT_8 are distributed into irreducible representations as follows:

$$\Gamma_{vib} = 3A_{1g}(R) + A_{2g}(in) + 4E_g(R) + 3T_{1g}(in) + 6T_{2g}(R) + 3A_{2u}(in) + 3E_u(in) + 6T_{1u}(IR) + 4T_{2u}(in) \quad (2)$$

where (IR) is IR active, (R) is Raman active and (in) is optically inactive, but all should be inelastic neutron scattering (INS) active. Of the 33 different fundamental vibrations of O_h HT_8, only six are IR active. In the case of the O_h $H@HT_8$, there is an additional IR-active T_{1u} mode. These frequencies are in good agreement with the experimental values. As indicated in Table 2, most features were similar between HT_8 and $H@HT_8$, except additional Si−O−Si bending appeared at 418 cm^{-1} in $H@HT_8$. IR data for $H@HT_8$ is not available because of the difficulty making measurements.

Isotropic Hyperfine Coupling Constant and Spin Density. Measurements of ESR spectra revealed that the hydrogen atom, the simplest of the atoms and free radicals, is encapsulated in the center of the D4R cage and is stable for many months at room temperature.[5,6] The isotropic hyperfine coupling constants (A_0 in Gauss) and the spin densities (ρ(0) in a.u.) are connected by the following equation:

$$A_0 = (8\pi/3)(g_e/g_0)g_N\beta_N\rho(0) \quad (3)$$

where (g_e/g_0) is the ratio of the g values of the free electron and the radical under consideration and is taken as unity hereafter; g_N and β_N are the nuclear g factor and the nuclear magneton, respectively; and ρ(0) is the spin density at the nucleus. Specifically, in the case of the H atom, eq 3 is described as $A_0 = 4469.8\rho(0)$, where A_0 is in MHz and ρ(0) is in a.u.[25,30] The values of ρ(0) and A_0 calculated by the three methods with two different basis sets are shown in Table 3. As the UHF, B3LYP, and MP2 wave functions applied here are not pure spin

eigenfunctions for the spin operator S^2, the so-called spin-contamination must be examined. In these calculations, however, the degree of spin-contamination is considered small, because the expected values of S^2 were in the range of 0.751−0.752, where 0.750 is the exact value for a doublet. The experimental value of A_0 for H@HT_8 is 1408.4 MHz[6] and that for the free hydrogen atom is 1420.4 MHz.[31] This shows that the effect of the HT_8 cage decreases the value of $\rho(0)$ of the trapped H atom in H@HT_8 slightly (about 0.8%) from that of the free H atom. While the decrease in $\rho(0)$ obtained from the B3LYP/Basis II//B3LYP/Basis I was 0.3%. Although this is not very good agreement, the evaluation of A_0 using the B3LYP/Basis II//B3LYP/Basis I is considered satisfactorily close to the experimental value. The use of fifteen Gaussian type functions (15 GTFs) as *s* functions of the trapped hydrogen atom is likely to contribute to the cusp condition.[24] The magnitudes of the total spin densities (ρ(total) /a.u.)obtained from the three calculation levels for the trapped H atom decreased in the order UHF/Basis II//UHF/Basis I (0.966), MP2/Basis II//B3LYP/Basis I (0.938), and B3LYP/Basis II//B3LYP/Basis I (0.884). The same order is also obtained using Basis I. For the system investigated, the B3LYP calculation seems to more properly introduce the electron correlation between the trapped H atom and the HT_8 cage by taking account of higher order correlations than the MP2 calculation.

References and Notes

(1) Frye, C. L.; Collins, W. T. *J. Am. Chem. Soc.* **1970**, *92*, 5586.
(2) Olesson, K. *Ark. Kemi* **1958**, *13*, 367.
(3) Hoebbel, D.; Wieker, W. *Z. Anorg. Allg. Chem.* **1971**, *384*, 43.
(4) Karge, H. G.; Weitkamp, J., Eds. *MOLECULAR SIEVES Science and Technology*; Springer: Berlin, 1998; Vol. 1.
(5) Sasamori, R.; Okaue, Y.; Isobe, T.; Matsuda, Y. *Science* **1994**, *265*, 1691.
(6) Deguchi, Y. Master's Thesis, Graduate School of Social and Cultural Studies, Kyushu University, 1996.
(7) Päch, M.; Stösser, R. *J. Phys. Chem. A* **1997**, *101*, 8360.
(8) Earley, C. W. *J. Phys. Chem.* **1994**, *98*, 8693.
(9) Tossell, J. A. *J. Phys. Chem.* **1996**, *100*, 14828.
(10) Xiang, K.-H.; Pandey, R.; Pernisz, U. C.; Freeman, C. *J. Phys. Chem. B* **1998**, *102*, 8704.
(11) Wichmann, D.; Jug, K. *J. Phys. Chem. B* **1999**, *103*, 10087.
(12) George, A. R.; Catlow, C. R. A. *Chem. Phys. Lett.* **1995**, *247*, 408.
(13) Tossell, J. A. *J. Phys. Chem. A* **1998**, *102*, 3368.
(14) Parr, R. G.; Yang, W. *Density-Functional Theory of Atoms and Molecules*; Oxford University Press: New York, 1989.
(15) Becke, A. D. *J. Chem. Phys.* **1993**, *98*, 5648.
(16) Pople, J. A.; Head-Gordon, M.; Fox, D. J.; Raghavachari, K.; Curtiss, L. A. *J. Chem. Phys.* **1989**, *90*, 5622.
(17) Curtiss, L. A.; Jones, C.; Trucks, G. W.; Raghavachari, K.; Pople, J. A. *J. Chem. Phys.* **1990**, *93*, 2537.
(18) Møller, C.; Plesset, M. S. *Phys. Rev.* **1934**, *46*, 618.
(19) Hariharan, P. C.; Pople, J. A. *Theor. Chim. Acta* **1973**, *28*, 213.
(20) Francl, M. M.; Pietro, W. J.; Hehre, W. J.; Binkley, J. S.; Gordon, M. S.; DeFrees, D. J.; Pople, J. A. *J. Chem. Phys.* **1982**, *77*, 3654.
(21) Krishnan, R.; Binkley, J. S.; Seeger, R.; Pople, J. A. *J. Chem. Phys.* **1980**, *72*, 650.
(22) Frisch, M. J.; Pople, J. A.; Binkley, J. S. *J. Chem. Phys.* **1984**, *80*, 3265.
(23) Pople, J. A.; Nesbet, R. K. *J. Chem. Phys.* **1954**, *22*, 571.
(24) Yamamoto, H.; Matsuoka, O. *Bull. Univ. Electro-Commun.* **1992**, *5*, 23.
(25) Frisch, M. J.; W. Trucks, G.; Schlegel, H. B.; Scuseria, G. E.; Robb, M. A.; Cheeseman, J. R.; Zakrzewski, V. G.; Montgomery, J. A., Jr.; Stratmann, R. E.; Burant, J. C.; Dapprich, S.; Millam, J. M.; Daniels, A. D.; N. Kudin, K.; Strain, M. C.; Farkas, O.; Tomasi, J.; Barone, V.; Cossi, M.; Cammi, R.; Mennucci, B.; Pomelli, C.; Adamo, C.; Clifford, S.; Ochterski, J.; Petersson, G. A.; Ayala, P. Y.; Cui, Q.; Morokuma, K.; Malick, D. K.; Rabuck, A. D.; Raghavachari, K.; Foresman, J. B.; Cioslowski, J.; Ortiz, J. V.; Stefanov, B. B.; Liu, G.; Liashenko, A.; Piskorz, P.; Komaromi, I.; Gomperts, R.; Martin, R. L.; Fox, D. J.; Keith, T.; Al-Laham, M. A.; Peng, C. Y.; Nanayakkara, A.; Gonzalez, C.; Challacombe, M.; Gill, P. M. W.; Johnson, B.; Chen, W.; Wong, M. W.; Andres, J. L.; Gonzalez, C.; Head-Gordon, M.; Replogle, E. S.; Pople, J. A. *Gaussian 98*, Revision A.5; Gaussian, Inc.: Pittsburgh, PA, 1998.
(26) Auf der Heyde, T. P. E.; Bürgi, H.-B.; Bürgy, H.; Törnroos, K. W. *Chimia* **1991**, *45*, 38.
(27) Bürgy, H.; Calzaferri, G.; Herren, D.; Zhdanov, A. *Chimia* **1991**, *45*, 3.
(28) Emsley, J. *The Elements*, 2nd ed.; Oxford University Press: New York, 1991.
(29) Forner, S. N.; Cohran, E. L.; Bowers, V. A.; Jen, C. K. *J. Chem. Phys.* **1960**, *32*, 963.
(30) Ohta, K.; Nakatsuji, H.; Hirao, K.; Yonezawa, T. *J. Chem. Phys.* **1980**, *73*, 1770.
(31) Kusch, P. *Phys. Rev.* **1955**, *100*, 1188.